AGU PUBLICATIONS

Geophysical Research Letters

RESEARCH LETTER

10.1002/2014GL059836

Key Points:
- Gravitational core-mantle coupling is 2–10 times weaker than previously thought
- Gravitational coupling is too weak to explain the 6 year length-of-day signal
- Based on LOD constraints, our results suggest an inner core viscosity consistent with recent mineral physics experiments

Supporting Information:
- Readme
- Text S1
- Table S1
- Table S2
- Table S3

Correspondence to:
C. J. Davies,
c.davies@leeds.ac.uk

Citation:
Davies, C. J., D. R. Stegman, and M. Dumberry (2014), The strength of gravitational core-mantle coupling, *Geophys. Res. Lett.*, *41*, 3786–3792, doi:10.1002/2014GL059836.

Received 8 APR 2014
Accepted 14 MAY 2014
Accepted article online 16 MAY 2014
Published online 5 JUN 2014

The strength of gravitational core-mantle coupling

Christopher J. Davies[1], Dave R. Stegman[2], and Mathieu Dumberry[3]

[1]School of Earth and Environment, University of Leeds, Leeds, UK, [2]Institute for Geophysics and Planetary Physics, Scripps Institution of Oceanography, University of California San Diego, La Jolla, California, USA, [3]Department of Physics, University of Alberta, Edmonton, Alberta, Canada

Abstract Gravitational coupling between Earth's core and mantle has been proposed as an explanation for a 6 year variation in the length-of-day (ΔLOD) signal and plays a key role in the possible superrotation of the inner core. Explaining the observations requires that the strength of the coupling, Γ, falls within fairly restrictive bounds; however, the value of Γ is highly uncertain because it depends on the distribution of mass anomalies in the mantle. We estimate Γ from a broad range of viscous mantle flow models with density anomalies inferred from seismic tomography. Requiring models to give a correlation larger than 70% to the surface geoid and match the dynamic core-mantle boundary ellipticity inferred from Earth's nutations, we find that $3 \times 10^{19} < \Gamma < 2 \times 10^{20}$ N m, too small to explain the 6 year ΔLOD signal. This new constraint on Γ has important implications for core-mantle angular momentum transfer and on the preferred mode of inner core convection.

1. Introduction

Convective flows in the Earth's mantle involve density variations with respect to its oblate, rotationally symmetric hydrostatic background state. These mass anomalies lead to distortion of the geoid—the topography of surfaces of constant gravitational potential—everywhere inside the Earth. The dominant perturbation occurs at spherical harmonic degree and order 2 and is associated with two antipodal thermochemical piles in the equatorial region of the lower mantle [e.g., *Simmons et al.*, 2007].

The fluid outer core also undergoes vigorous convection, though the associated density anomalies are much smaller than those involved in mantle convection [*Stevenson*, 1987]. Departures from hydrostatic equilibrium in the outer core are very small, and the hydrostatic core density structure (and associated geoid) must deform to coincide with that imposed by the mantle. If the inner core is not convecting, which appears likely at least at the present time [*Buffett*, 2009; *Gubbins et al.*, 2013], then its density structure should also align with that of the mantle. This requires the inner core viscosity to be lower than that of the mantle, which is supported by recent mineral physics experiments [*Gleason and Mao*, 2013] and also by inference from nutation observations [*Koot and Dumberry*, 2011].

Any longitudinal misalignment between the density fields of the inner core and mantle, e.g., due to torques on the inner core arising from the geodynamo process [*Buffett and Glatzmaier*, 2000; *Aubert and Dumberry*, 2011], results in a restoring gravitational torque between the two [*Buffett*, 1996]. The amplitude of the torque is proportional to the misalignment angle between the two bodies and to a coupling constant, Γ, which depends on the distribution of mass anomalies in the mantle. If the timescale for deformation of the inner core, τ, is relatively short, its density field can realign to that of the mantle via deformation rather than rotation [*Buffett*, 1997], and the effective strength of the gravitational torque is reduced.

Gravitational coupling allows transfer of angular momentum between the core and mantle. It has been proposed that the 6 year periodic variation in length of day (ΔLOD) [*Holme and de Viron*, 2013] may represent the signature of the free mode of mantle-inner core gravitational (MICG) oscillation [*Mound and Buffett*, 2006]. If this latter hypothesis is correct then Γ cannot depart significantly from $\Gamma_{\mathrm{MICG}} = 3 \times 10^{20}$ N m and the very observation of this mode implies that τ must be larger than 6 years.

Gravitational coupling also bears directly on the seismically inferred superrotation of the inner core (see *Souriau* [2007] for a review). If $\Gamma = \Gamma_{\mathrm{MICG}}$ gravitational coupling should prevent such differential rotation, unless the inner core can viscously deform on a short (~0.1–1 year) timescale [*Buffett*, 1997] which conflicts with $\tau > 6$ years. The strong gravitational coupling suggested by $\Gamma = \Gamma_{\mathrm{MICG}}$ and $\tau > 6$ years implies that

the inner core and mantle should remain aligned on a time average, and the seismic signal may instead capture a fragment of inner core oscillations [*Tkalčić et al.*, 2013]. However, a strong gravitational coupling is also problematic in this scenario because it induces mantle oscillations that could exceed the observed decadal ΔLOD [e.g., *Dumberry and Mound*, 2010]. Full treatment of the angular momentum problem requires consideration of electromagnetic (EM) coupling at the core-mantle boundary (CMB), but for typical estimates of the latter, the observed ΔLOD constrains the product $\Gamma\tau$ to be $< 5 \times 10^{19}$ N m yr [*Dumberry and Mound*, 2010]. This estimate is based on restricting mantle oscillations at long (millennial) timescales; at periods of 80–100 years, the inner core is less efficient at entraining the mantle because of the latter's large moment of inertia and a slightly less restrictive constraint of $\Gamma\tau \lesssim 2 \times 10^{20}$ N m yr applies, similar to that inferred by *Aubert* [2013] based on the ΔLOD generated in geodynamo simulations.

The strength of Γ is crucial for understanding angular momentum transfer between the core and mantle and the rotational dynamics of the inner core. Moreover, better knowledge of Γ will improve constraints on the viscosity of the inner core. The latter is an important parameter for understanding past or present convection in the inner core and possible internal deformation that could explain its complex seismic signature [*Deguen*, 2012]. Without a definitive observational constraint on Γ, it must be determined by explicit calculation. The only such calculation to date is due to *Buffett* [1996]. He used two models of the mantle density obtained by solving a Stokes equation for the viscous flow driven by static density anomalies inferred from seismic tomography and obtained $\Gamma \approx 3 \times 10^{20}$ N m. Though this would be consistent with a 6 year MICG mode, the viscous flow calculation depends on highly uncertain quantities which lead to large uncertainties in Γ.

In this paper we conduct a suite of 309 viscous flow calculations to place robust bounds on the value of Γ. A description of the model and a justification of our chosen input parameters are given in section 2. In section 3 we show the dependence of Γ on the model inputs and select calculations for further study if they provide a satisfactory fit to the surface geoid and the dynamic ellipticity of the CMB. Discussion is presented in section 4 and conclusions in section 5.

2. Model

The axial gravitational torque exerted on the inner core by the mantle is given by

$$\Gamma_g = \Gamma\phi, \tag{1}$$

where ϕ is the misalignment angle between mantle and inner core density fields (assumed small) and Γ measures the strength of the coupling. Defining the topography of the geoid at the CMB by

$$q(\theta,\phi) = \sum_{l=1}^{\infty}\sum_{m=-l}^{l} A_l^m Y_l^m(\theta,\phi), \tag{2}$$

where the $Y_l^m(\theta,\phi)$ are fully normalized spherical harmonics of degree l and order m and A_l^m are (complex) coefficients, *Dumberry* [2010] shows that Γ can be expressed as

$$\Gamma = 2g_i r_i^2(\rho_s - \rho_f)\sum_{l=2}^{\infty}\sum_{m=1}^{l} m^2\left(\frac{r_i}{r_o}\right)^{(2l-2)}\left|A_l^m\right|^2. \tag{3}$$

(see *Dumberry* [2008] for a detailed discussion). Here $r_o = 3485$ km is the CMB radius, $r_i = 1221$ km is the inner core boundary (ICB) radius, $g_i \approx 4.4$ m s^{-2} is gravity at the ICB, $\rho_s = 12730$ kg m^{-3} is the inner core density (assumed uniform), and $\rho_f = 12160$ kg m^{-3} is the density of the fluid core at the ICB. In deriving (3), density anomalies associated with inner and outer core convection have been neglected, and the limit of large τ has been assumed so the inner core is effectively a rigid body. We concentrate on the $l = m = 2$ component of (3), which is well known to be the largest contribution to Γ [*Buffett*, 1996]. The primary uncertainty in determining Γ is due to A_l^m.

We calculate A_l^m using the code HC available at http://www.geodynamics.org/cig/software/hc, which uses a propagation matrix solution method to solve for incompressible mantle flow within a layered stack of spherical shells [*Hager and O'Connell*, 1981]. A viscosity profile $\mu(r)$ is prescribed such that each radial shell has a Newtonian viscosity. The body forces that drive motion are prescribed by relating seismic velocity

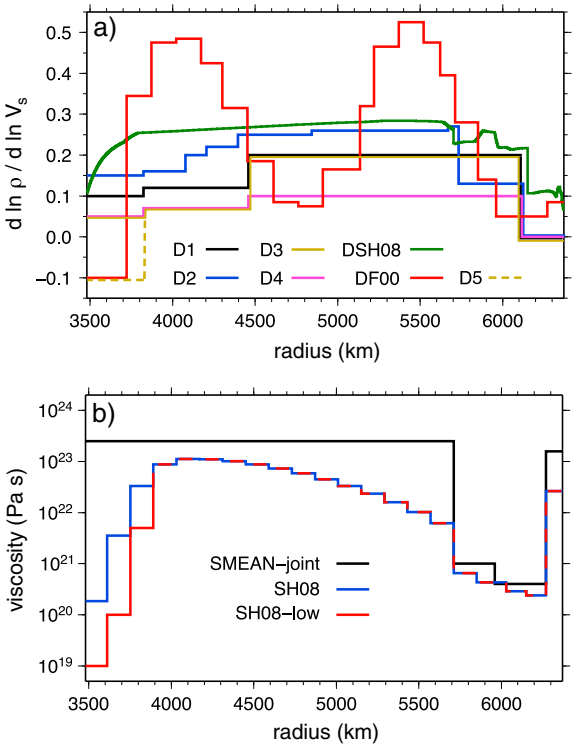

Figure 1. Radial profiles of (a) $d \ln \rho / d \ln V_s$ and (b) μ used in this work. See text for details.

anomalies to density anomalies using a scaling factor, which can also vary in radius r. The velocity boundary condition at the CMB is stress-free, and the surface velocity condition can be no-slip, free-slip (fs), or prescribed by plate motions. Previous studies have shown that models of mantle flow driven by prescribed body forces can explain up to 80% of the observed geoid [e.g., *Simmons et al.*, 2006]. Moreover, the method is fast, allowing many simulations to be undertaken.

If density anomalies have a purely thermal origin then the scaling factor between seismic velocity and density is $d \ln \rho / d \ln V_s$ where ρ is the nonhydrostatic density and V_s the seismic shear velocity anomalies with respect to a 1-D average profile, which we take as PREM [*Dziewonski and Anderson*, 1981]. There is also evidence that seismic velocity variations reflect chemical heterogeneity, specifically in two large low shear velocity provinces (LLSVPs) in the bottom ~300 km of the mantle below Africa and the central Pacific [e.g., *Garnero and McNamara*, 2008]. *Steinberger and Holme* [2008] showed that the presence of chemically distinct (heavier) LLSVPs significantly reduce CMB topography; the associated change in the geoid could then also affect Γ. We model chemically distinct LLSVPs following modeling case C of *Steinberger and Holme* [2008]. The parameter k_1, which determines the amplitude of nonthermal density heterogeneity in *Steinberger and Holme* [2008], is prescribed such that regions in the bottom two layers of a given tomography model with velocity anomaly below −1% are denser by a few percent compared to the surrounding mantle [*Garnero and McNamara*, 2008]. We consider $k_1 = 0$ (purely thermal density anomalies) and $k_1 = 2$ or 5 which gives a difference between the maximum density in the piles and ambient mantle of 1–6% depending on the tomography model and $d \ln \rho / d \ln V_s$. The difference between the minimum and maximum density within the LLSVPs varies between 0.5% and 5% in our suite of models, and the LLSVPs are generally most dense at the edges (unless $d \ln \rho / d \ln V_s$ is negative in the lowermost mantle). See supporting information for more details.

In the following section we establish the dependence of Γ on the five main inputs to HC: surface boundary condition, seismic tomography model, $\mu(r)$, $d \ln \rho / d \ln V_s$, and k_1. We consider the three velocity boundary conditions described above with the horizontal divergence of plate velocities from *DeMets et al.* [1990]. Nine seismic shear velocity models are included: NGRAND, S20RTS, SAW24B16, SB4L18, TX2008, S362WMANI, HMSL, LH08, and SMEAN (see *Becker and Boschi* [2002] and Table S1 in the supporting information for additional details of these models). We consider nine $d \ln \rho / d \ln V_s$ profiles (Figure 1), two of which use a constant scaling factor given by $d \ln \rho / d \ln V_s = 0.1$ or 0.25. The profile DSH08 is from *Steinberger and Holme* [2008], while the profiles D1–D4 are based on the study of *Karato and Karki* [2001], which assumes dominance of thermal over compositional effects. The profile DF00 [*Forte et al.*, 1994] is characterized by two broad peaks and a sign change in the bottom ~300 km of the mantle. The final $d \ln \rho / d \ln V_s$ profile is D5, which follows profile D3 everywhere except the bottom ~300 km of the mantle, where its sign is changed to match profile DF00. Figure 1 also shows the three viscosity profiles used in this work: SMEAN-joint [*Soldati et al.*, 2009], SH08 [*Steinberger and Holme*, 2008], and SH08-low. SMEAN-joint is characterized by a region of low viscosity in the upper 700 km and a flat profile below with a maximum value of $\mu(r) = 3 \times 10^{23}$ Pa s. SH08 also has a low viscosity upper 700 km, but $\mu(r)$ rises more gradually with depth than in SMEAN-joint and reaches a maximum of 10^{23} Pa s before falling sharply by 3 orders of magnitude in the bottom ~300 km. SH08-low is a modified version of SH08 incorporating the $O(10^4)$ viscosity drop in the bottom ~300 km proposed by *Ammann et al.* [2010] for post-perovskite at lower mantle conditions.

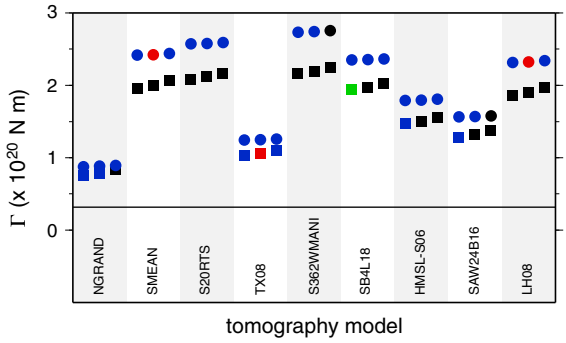

Figure 2. Gravitational coupling constant Γ for different seismic tomography models using free-slip (circles) and plates (squares) boundary conditions. (left to right) Results for k_1 = 0, 2, and 5 are given for each tomography model. Colors indicate whether models successfully match the constraints on the geoid ($C > 70$) and dynamic ellipticity of the CMB ($-480 \le h_2^0 \le -320$): red indicates that both C and h_2^0 are satisfied; blue, only C is satisfied; green, only h_2^0 is satisfied; and black, neither. The density scaling profile is D1, and the viscosity profile is SH08.

When considering the success of a given model, we note that the aforementioned profiles of d ln ρ/d ln V_s and μ have all been constrained to match certain observational and experimental data in some manner (e.g., through an inversion procedure). Further constraints can be added using outputs of the mantle flow model, specifically the gravitational potential. We first require that the correlation C between synthetic and observed surface geoid is > 70%. This value is chosen so that the criterion is not too restrictive; less than 10% of models have $C > 80\%$. We employ a second criterion based on the dynamic ellipticity of the CMB, which we denote by h_2^0. Depending on the strength of EM coupling at the CMB, inference from Earth's nutations suggest that $-465 \le h_2^0 \le -393$ m [*Koot et al.*, 2010]. We require that successful models satisfy $-480 \le h_2^0 \le -320$ m, which allows for uncertainty in h_2^0 due to the coupling mechanism.

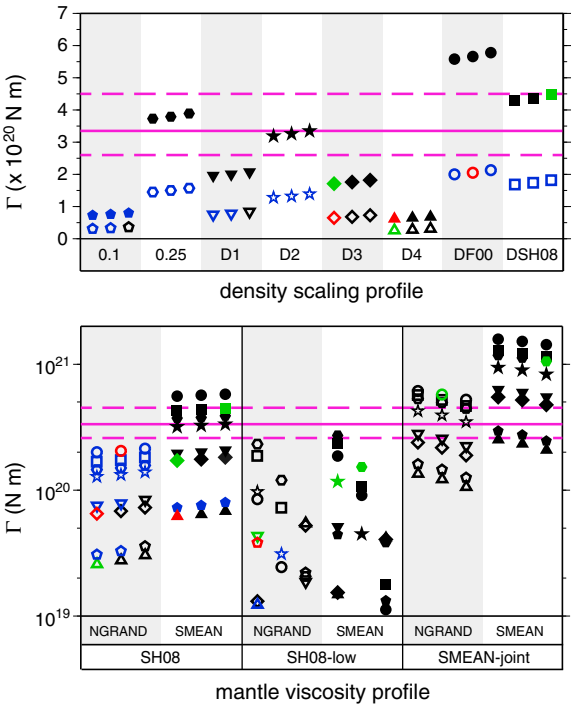

Figure 3. Gravitational coupling constant Γ for different (top) density scaling and (bottom) viscosity profiles. Symbols identify the density scaling profiles; open (filled) symbols denote the NGRAND (SMEAN) tomography model. Results for k_1=0, 2, and 5 (left to right) are given for each set of model parameters. Colors indicate whether models successfully match the constraints on the geoid ($C > 70$) and dynamic ellipticity of the CMB ($-480 \le h_2^0 \le -320$): red indicates that both C and h_2^0 are satisfied; blue, only C is satisfied; green, only h_2^0 is satisfied; and black, neither. The purple solid line indicates the value of Γ that matches a MICG free mode period of 5.8 years (±0.8 years: dashed lines). All models have plate motions imposed on the upper boundary. The viscosity profile used in Figure 3 (top) is SH08.

3. Results

The suite of 309 models conducted for this study is summarized in the supporting information. We find significant variations in h_2^0, C, and Γ: for $k_1 = 0$ (purely thermal density variations) $-2500 \le h_2^0 \le -27$ m, $0.46 \le C \le 0.83$, and $1.23 \times 10^{19} \le \Gamma \le 1.58 \times 10^{21}$ N m.

The dependence of Γ on the surface boundary condition and tomography model is shown in Figure 2 for the D1 profile of d ln ρ/d ln V_s, the SH08 viscosity profile, and our three choices of k_1. Γ varies by as much as a factor 3 between the different models, with its value being the lowest for the NGRAND model. The range of Γ reflects the integrated differences between tomography models.

Figure 3 shows the dependence of Γ on d ln ρ/d ln V_s and $\mu(r)$ for the NGRAND and SMEAN tomography models. We have carried out calculations for all tomography models (see supporting information); these two models yield Γ at the upper and lower ends of the values in our suite of calculations, all other factors being equal. Increasing d ln ρ/d ln V_s increases Γ because the same V_s anomalies are translated into stronger density variations, although the value of Γ does

Table 1. Summary of Models That Fulfill the Criteria $C > 70\%$ and $-480 \leq h_2^0 \leq -320$ m for $k_1 = 0$ (Top Section) and $k_1 = 2$ (Bottom Section)[a]

d ln ρ/d ln V_s	Tomography Model	Surface BC	μ Profile	Γ	h_2^0	C
0.1	NGRAND	plates	SH08-low	3.828×10^{19}	−330.331	0.750
D3	SMEAN	fs	SH08	2.061×10^{20}	−450.508	0.789
D3	NGRAND	plates	SH08	6.503×10^{19}	−472.526	0.724
D4	SMEAN	plates	SH08	6.184×10^{19}	−372.176	0.705
D4	TX2008	plates	SH08	3.476×10^{19}	−439.994	0.719
0.1	NGRAND	fs	SH08	3.098×10^{19}	−406.045	0.784
0.1	SMEAN	fs	SH08	8.086×10^{19}	−343.877	0.817
D1	LH08	fs	SH08	2.325×10^{20}	−341.814	0.822
D1	SMEAN	fs	SH08	2.423×10^{20}	−337.044	0.804
D1	TX2008	plates	SH08	1.061×10^{20}	−452.301	0.763
DF00	NGRAND	plates	SH08	2.052×10^{20}	−448.688	0.776

[a]We did not find any model that satisfied both criteria for $k_1 = 5$. d ln ρ/d ln V_s (kg s m^{-4}) is the scaling between shear velocity and density and μ (Pa s) is the mantle viscosity; the profiles are shown in Figure 1. The tomography models are NGRAND [*Grand et al.*, 1997; *Becker and Boschi*, 2002], TX2008 [*Simmons et al.*, 2006], and SMEAN [*Becker and Boschi*, 2002]. For the surface boundary condition "fs" refers to a free-slip condition while "plates" indicates that the horizontal divergence of plate velocities are prescribed [*DeMets et al.*, 1990]. Γ (N m) is the strength of the gravitational coupling defined in (3) and h_2^0 (m) is the magnitude of the spherical harmonic degree 2 and order 0 component of the CMB topography. C refers to the correlation between model and observed surface geoid.

not seem to be very sensitive to changes in d ln ρ/d ln V_s over particular depth ranges. For instance, the value of Γ is largest with the DF00 profile because d ln ρ/d ln V_s is high over large depth ranges in the mantle, even though d ln ρ/d ln V_s changes sign and becomes negative near the base of the mantle. High mantle viscosity gives high Γ because internal deformations in the mantle are relatively weak; significant geoid topography is induced at the CMB in response to the static density distribution. As with d ln ρ/d ln V_s, the value of Γ seems sensitive to changes in $\mu(r)$ at all depths. The main point is that Γ varies significantly with d ln ρ/d ln V_s and $\mu(r)$.

Allowing for chemical heterogeneity in the lower ~300 km of the mantle changes Γ, but whether it increases or decreases depends on the viscosity profile. As Figure 3 shows, Γ increases with increasing k_1 for the SH08 profile, while the reverse is observed for the SMEAN-joint profile. With a very low viscosity in the lower mantle (SH08-low), Γ can decrease by as much as a few orders of magnitude for an increase in chemical heterogeneity. This is because the region near the CMB is less able to support radial viscous stresses and therefore pressure gradients arising from lateral density variations will preferentially drive horizontal flow, resulting in a correspondingly smaller CMB topography and associated geoid amplitude. For the SH08 viscosity profile we also observe that increasing k_1 strongly decreases the excess CMB ellipticity h_2^0 and leaves C almost unaffected (see supporting information), in agreement with the results of *Steinberger and Holme* [2008].

Γ can vary by a few orders of magnitude depending on the preferred density scaling and viscosity profile of the mantle (Figure 3 and supporting information). However, a much narrower range of values is found when we further constrain the mantle flow model to be in good agreement with the surface geoid. For $k_1 = 0$ (purely thermal density variations), 70 models remain when we require $C > 60\%$ (68 with $k_1 = 2$ and 57 with $k_1 = 5$), which falls to 42 when we require $C > 70\%$ (38 with $k_1 = 2$ and 27 with $k_1 = 5$) and 6 when we require $C > 80\%$ (8 with $k_1 = 2$ and 6 with $k_1 = 5$). We do not expect C to be very high because of the limitations in the viscous model. Henceforth, we focus on models with $C > 70\%$, which provides a relatively strict constraint while still leaving plenty of models to analyze. An even more restricted set of models match the constraint $-480 \leq h_2^0 \leq -320$ m on the dynamic ellipticity of the CMB: 14 models with $k_1 = 0$, 11 models with $k_1 = 2$ and two models with $k_1 = 5$.

Models that satisfy the constraint $C > 70\%$ are denoted by blue symbols in Figures 2 and 3 and Tables S1–S3, models that match $-480 \leq h_2^0 \leq -320$ m by green symbols, while models that satisfy both constraints are shown in red. For $k_1 = 0$ ($k_1 = 2$) we found only five (six) models that pass both constraints on h_2^0 and $C > 70\%$; these are listed in Table 1. No successful models are found for $k_1 = 5$. When $C > 80\%$, we found two models that comply with both constraints with $k_1 = 2$ and no models with $k_1 = 0$.

The range of Γ for our successful models (Table 1) is $3 \times 10^{19} < \Gamma < 2 \times 10^{20}$ N m. Ignoring the nutation constraint on h_2^0 shows that the majority of the models with $C > 70\%$ (33 of 42 for $k_1 = 0$, 27 of 38 for $k_1 = 2$, and 20 of 27 for $k_1 = 5$) remain within these bounds. Successful models have a weak density-V_s scaling throughout the mantle and a reduced viscosity in the lower mantle; however, a $\mu(r)$ that is too low in the lower mantle tends to cause models to fail the constraint on h_2^0.

4. Discussion

Explaining the observed 5.8 ± 0.8 year periodic ΔLOD signal [*Holme and de Viron*, 2013] by the free mode of mantle-inner core gravitational (MICG) oscillation [*Mound and Buffett*, 2006] requires $2.6 \times 10^{20} < \Gamma < 4.5 \times 10^{20}$ N m. Although we do find many models that match this range of Γ (see Figure 3), these models tend to have a poor fit to the geoid. Models that fit the geoid well tend to fall within the range of Γ of our successful models (Table 1). Indeed, relaxing the nutation constraint and still requiring that $C > 70\%$ shows that the above condition on Γ is satisfied by only 3 of 42 models with $k_1 = 0$, 3 of 38 models with $k_1 = 2$, and 2 of 27 models with $k_1 = 5$. These conclusions are based on a model of mantle flow that contains certain limitations in terms of the physics (buoyancy forces are prescribed rather than calculated, and physical properties only vary in the radial direction) and uncertainties in the inputs (e.g., mantle viscosity). It is also possible that successful models meeting our criteria and yielding a Γ within the range needed to explain the 6 year ΔLOD signal lie in unsampled regions of parameter space; however, given that none of our 309 models meet these conditions it seems that such models will require a very specific set of mantle properties and we have no basis to argue that such conditions are favored. With these caveats in mind, our results suggest it is unlikely that the 6 year ΔLOD can be explained by the MICG mode.

Our values of Γ give support to an alternative suggestion that the 6 year signal represents angular momentum exchange between fast torsional oscillations in the fluid core and the mantle [*Gillet et al.*, 2010]. Though the nature of the torque between these waves and the mantle remains uncertain, this scenario relieves the constraint that $\Gamma = \Gamma_{\mathrm{MICG}}$. Using our new estimate of Γ gives a MICG period of 7–18 years (which would be lengthened if viscous dissipation occurs on a short timescale of a few years, as we suggest below), suggesting that the MICG mode may be related to longer period ΔLOD signals.

Ensuring that gravitational coupling does not lead to ΔLOD at 80–100 year periods that are larger than observed imposes a constraint that $\Gamma\tau \lesssim 2 \times 10^{20}$ N m yr [*Dumberry and Mound*, 2010; *Aubert*, 2013], which yields an upper bound on τ of 1–6 years using our best estimate of Γ. Using the mapping of *Buffett* [1997], which was based on a fairly high inner core rotation rate [*Song and Richards*, 2006], gives an upper bound for the inner core viscosity of approximately 3×10^{17} Pa s, compatible with estimates of 10^{15}–10^{18} Pa s obtained from recent mineral physics experiments [*Gleason and Mao*, 2013]. We note, however, that estimates of the inner core viscosity are still subject to large uncertainties with some studies reporting values of 10^{20}–10^{22} Pa s [e.g., *Yoshida et al.*, 1996; *Reaman et al.*, 2011].

The inner core viscosity has important implications for its mode of convection. *Deguen* [2012] estimated that the preferred mode of convection (if the inner core does indeed convect) depends on the parameter $\mathcal{P} = \tau_\phi/\tau$, where $\tau_\phi \approx 1000$ years is a timescale of phase change at the ICB. For the inner core to undergo a translational mode of convection requires $\mathcal{P} \lesssim 20$, otherwise it is instead in a plume convection regime [*Deguen*, 2012]. Our estimate of $\tau \lesssim 6$ years, implies $\mathcal{P} \gtrsim 150$, firmly in the plume regime. This has important implications because the translational mode has been proposed to explain some aspects of the inner core's hemispherical seismic structure [*Monnereau et al.*, 2010; *Alboussière et al.*, 2010]. Further, the degree 1 equatorial buoyancy flux at the ICB implied by such a scenario can significantly influence fluid flow in the outer core [*Davies et al.*, 2013] and may explain some features of the magnetic field variation on long [*Olson and Deguen*, 2012] and short [*Aubert*, 2013] timescales. For the inner core to be in a translation regime, either τ_ϕ must be much smaller than 1000 years or τ must be much larger than our above estimate, or both. The latter could be accomplished by a large unaccounted torque at the CMB which can restrict the amplitude of mantle oscillations.

5. Conclusions

The main result of this study is a revised estimate of the strength of gravitational coupling between the inner core and mantle, which is a factor of 2–10 lower than the only previous estimate obtained by direct calculation [*Buffett*, 1996]. To arrive at this result, we have constrained the outputs of our chosen mantle flow

model to (1) provide a > 70% correlation to the surface geoid and (2) match the dynamic CMB topography inferred from Earth's nutations. Future studies of ΔLOD, mantle-core coupling mechanisms, and inner core convection, translation, or oscillation will benefit from this improved estimate of Γ.

Acknowledgments
C.D. is supported by a Natural Environment Research Council personal fellowship, NE/H01571X/1. M.D. is supported by a Discovery grant from NSERC/CSRNG. D.S. acknowledges support from NSF grant EAR-1361228. We thank the Computational Infrastructure for Geodynamics (CIG) for distributing HC and two anonymous reviewers for thorough and constructive comments.

The Editor thanks Bernhard Steinberger and an anonymous reviewer for their assistance in evaluating this paper.

References

Alboussière, T., R. Deguen, and M. Melzani (2010), Melting-induced stratification above the Earth's inner core due to convective translation, *Nature*, *466*, 744–747.
Ammann, M., J. Brodholt, J. Wookey, and D. Dobson (2010), First-principles constraints on diffusion in lower-mantle minerals and a weak D″ layer, *Nature*, *465*, 462–465.
Aubert, J. (2013), Flow throughout the Earth's core inverted from geomagnetic observations and numerical dynamo models, *Geophys. J. Int.*, *192*, 537–556.
Aubert, J., and M. Dumberry (2011), Steady and fluctuating inner core rotation in numerical geodynamo models, *Geophys. J. Int.*, *184*, 162–170.
Becker, T., and L. Boschi (2002), A comparison of tomographic and geodynamic mantle models, *Geochem. Geophys. Geosyst.*, *3*(1), 1003, doi:10.1029/2001GC000168.
Buffett, B. (1996), Gravitational oscillations in the length of day, *Geophys. Res. Lett.*, *23*, 2279–2282.
Buffett, B. (1997), Geodynamic estimates of the viscosity of Earth's inner core, *Nature*, *388*, 571–573.
Buffett, B. (2009), Onset and orientation of convection in the inner core, *Geophys. J. Int.*, *179*, 711–719.
Buffett, B., and G. Glatzmaier (2000), Gravitational braking of inner-core rotation in geodynamo simulations, *Geophys. Res. Lett.*, *27*, 3125–3128.
Davies, C., L. Silva, and J. Mound (2013), On the influence of a translating inner core in models of outer core convection, *Phys. Earth Planet. Inter.*, *214*, 104–114.
Deguen, R. (2012), Structure and dynamics of Earth's inner core, *Earth Planet. Sci. Lett.*, *333-334*, 211–225.
DeMets, C., R. Gordon, D. Argus, and S. Stein (1990), Current plate motions, *Geophys. J. Int.*, *101*, 425–478.
Dumberry, M. (2008), Gravitational torque on the inner core and decadal polar motion, *Geophys. J. Int.*, *172*, 903–920.
Dumberry, M. (2010), Gravitationally driven inner core differential rotation, *Earth Planet. Sci. Lett.*, *297*, 387–394.
Dumberry, M., and J. Mound (2010), Inner core-mantle gravitational locking and the super-rotation of the inner core, *Geophys. J. Int.*, *181*, 806–817.
Dziewonski, A., and D. Anderson (1981), Preliminary reference Earth model, *Phys. Earth Planet. Inter.*, *25*, 297–356.
Forte, A., R. Woodward, and A. Dziewonski (1994), Joint inversions of seismic and geodynamic data for models of three-dimensional mantle heterogeneity, *J. Geophys. Res.*, *99*, 21,857–21,877.
Garnero, E., and A. McNamara (2008), Structure and dynamics of Earth's lower mantle, *Science*, *320*, 626–628.
Gillet, N., D. Jault, E. Canet, and A. Fournier (2010), Fast torsional waves and strong magnetic field within the Earth's core, *Nature*, *465*, 74–77.
Gleason, A., and W. Mao (2013), Strength of iron at core pressures and evidence for a weak Earth's inner core, *Nat. Geosci.*, *6*, 571–574.
Grand, S. P., R. van der Hilst, and S. Widiyantoro (1997), Global seismic tomography: A snapshot of convection in the Earth, *GSA Today*, *7*, 1–7.
Gubbins, D., D. Alfé, and C. Davies (2013), Compositional instability of Earth's solid inner core, *Geophys. Res. Lett.*, *40*, 1084–1088, doi:10.1002/grl.50186.
Hager, B., and R. O'Connell (1981), A simple global model of plate dynamics and mantle convection, *J. Geophys. Res.*, *86*, 4843–4867.
Holme, R., and O. de Viron (2013), Characterization and implications of intradecadal variations in length of day, *Nature*, *499*, 202–204.
Karato, S.-I., and B. Karki (2001), Origin of lateral variation of seismic wave velocities and density in the deep mantle, *J. Geophys. Res.*, *106*, 21,771–21,783.
Koot, L., and M. Dumberry (2011), Viscosity of the Earth's inner core: Constraints from nutation observations, *Earth Planet. Sci. Lett.*, *308*, 343–349.
Koot, L., M. Dumberry, A. Rivoldini, O. de Viron, and V. Dehant (2010), Constraints on the coupling at the core-mantle and inner core boundaries inferred from nutation observations, *Geophys. J. Int.*, *182*, 1279–1294.
Monnereau, M., M. Calvet, L. Margerin, and A. Souriau (2010), Lopsided growth of Earth's inner core, *Science*, *328*, 1014–1017.
Mound, J., and B. Buffett (2006), Detection of a gravitational oscillation in length-of-day, *Earth Planet. Sci. Lett.*, *243*, 383–389.
Olson, P., and R. Deguen (2012), Eccentricity of the geomagnetic dipole caused by lopsided inner core growth, *Nat. Geosci.*, *5*, 565–569.
Reaman, D., G. Daehn, and W. Panero (2011), Predictive mechanism for anisotropy development in the Earth's inner core, *Earth Planet. Sci. Lett.*, *312*, 437–442.
Simmons, N., A. Forte, and S. Grand (2006), Constraining mantle flow with seismic and geodynamic data: A joint approach, *Earth Planet. Sci. Lett.*, *246*, 109–124.
Simmons, N., A. Forte, and S. Grand (2007), Thermochemical structure and dynamics of the African superplume, *Geophys. Res. Lett.*, *34*, L02301, doi:10.1029/2006GL028009.
Soldati, G., L. Boschi, F. Deschamps, and D. Giardini (2009), Inferring radial models of mantle viscosity from gravity (GRACE) data and an evolutionary algorithm, *Phys. Earth Planet. Inter.*, *176*, 19–32.
Song, X., and P. Richards (2006), Seismological evidence for differential rotation of the Earth's inner core, *Nature*, *382*, 221–224.
Souriau, A. (2007), Deep Earth structure—The Earth's cores, in *Treatise on Geophysics*, vol. 1, edited by G. Schubert, B. Romanowicz, and A. Dziewonski, chap. 19, pp. 655–693, Elsevier, Amsterdam, Netherlands.
Steinberger, B., and R. Holme (2008), Mantle flow models with core-mantle boundary constraints and chemical heterogeneities in the lowermost mantle, *J. Geophys. Res.*, *113*, B05403, doi:10.1029/2007JB005080.
Stevenson, D. (1987), Limits on lateral density and velocity variations in the Earth's outer core, *Geophys. J. Int.*, *88*, 311–319.
Tkalčić, H., M. Young, T. Bodin, S. Ngo, and M. Sambridge (2013), The shuffling rotation of the Earth's inner core revealed by earthquake doublets, *Nat. Geosci.*, *6*, 497–502.
Yoshida, S., I. Sumita, and M. Kumazawa (1996), Growth model of the inner core coupled with the outer core dynamics and the resulting elastic anisotropy, *J. Geophys. Res.*, *101*, 28,085–28,103.